Dynamic motility selection drives population segregation in a bacterial swarm

Wenlong Zuo[a,b] and Yilin Wu (吴艺林)[a,b,1]

[a]Department of Physics, The Chinese University of Hong Kong, Shatin, New Territories, Hong Kong, People's Republic of China; and [b]Shenzhen Research Institute, The Chinese University of Hong Kong, Shenzhen 518057, People's Republic of China

Edited by E. Peter Greenberg, University of Washington, Seattle, WA, and approved January 22, 2020 (received for review October 11, 2019)

Population expansion in space, or range expansion, is widespread in nature and in clinical settings. Space competition among heterogeneous subpopulations during range expansion is essential to population ecology, and it may involve the interplay of multiple factors, primarily growth and motility of individuals. Structured microbial communities provide model systems to study space competition during range expansion. Here we use bacterial swarms to investigate how single-cell motility contributes to space competition among heterogeneous bacterial populations during range expansion. Our results revealed that motility heterogeneity can promote the spatial segregation of subpopulations via a dynamic motility selection process. The dynamic motility selection is enabled by speed-dependent persistence time bias of single-cell motion, which presumably arises from physical interaction between cells in a densely packed swarm. We further showed that the dynamic motility selection may contribute to collective drug tolerance of swarming colonies by segregating subpopulations with transient drug tolerance to the colony edge. Our results illustrate that motility heterogeneity, or "motility fitness," can play a greater role than growth rate fitness in determining the short-term spatial structure of expanding populations.

bacterial swarming | flagellar motility | antibiotic tolerance | adaptive stress response | collective motion

Population expansion in space (or range expansion) is widespread in nature and in clinical settings; examples include migration of alien species (1), cancer invasion (2), and microbial dispersal (3, 4). As phenotypic and genetic heterogeneity often exist in populations, space competition among the heterogeneous subpopulations during range expansion is essential to niche dynamics and to the evolutionary dynamics of genetic mutations (5, 6). Such space competition may involve the interplay of multiple factors, primarily growth and motility (or dispersal rate) (7–9). Understanding how growth and motility control the dynamics of space competition among subpopulations may provide insights on diverse range-expansion processes.

Structured microbial communities offer tractable model systems to study range expansion (8, 10–13). In particular, with convenience to manipulate individual cells' motility or collective dispersal rate, microbial communities are well suited to study the role of motility in space competition among subpopulations. Indeed, experiments with engineered microbial communities demonstrated the paradoxical phenomenon that dispersal could reduce population spread [i.e., the Allee effect (14)] (8, 15); recent studies have revealed important insights on how trade-off between growth and motility controls the long-term dynamics of space competition in expanding microbial communities (12, 13). In these studies the role of motility in space competition was addressed over long time scales that span many generations, and individual motility was often coupled to growth. At shorter time scales before growth selection has taken effect, it is usually believed that individual cells' motility promotes population mixing and blurs the boundaries between subpopulations (16, 17). However, microbial communities often consist of subpopulations with different motilities (18, 19). It is unclear how motility heterogeneity may affect the dynamics of population structure during range expansion.

Here we discovered that motility heterogeneity can promote the spatial segregation of subpopulations in structured microbial communities via a dynamic motility selection mechanism. Our finding was made with swarming bacterial colonies (20–22). By tracking single-cell motion pattern and measuring population structure during swarm expansion, we uncover a linear relation between single-cell speed and the motion bias toward the swarm edge, which presumably arises from physical interactions in the dense swarm. This emergent motion pattern results in a dynamic motility selection process in dense swarms that causes spatial segregation of subpopulations with different motilities. We further showed that swarms may employ this dynamic motility selection process to segregate subpopulations with transient drug tolerance to the swarm edge, thereby sustaining colony expansion into regions with lethal antibiotic concentrations.

The empirical relation between cell speed and motion bias we uncovered offers a unique mechanism via which individual motility may contribute to space competition among heterogeneous microbial populations during range expansion. Like in other organisms, space competition in microbial communities is crucial to population survival and interaction. Our findings are therefore relevant to microbial stress response and ecology. The findings are also relevant to range expansion in other biological systems, such as tumor invasion and collective stress tolerance of cancer cells in densely packed environments (2, 23).

Significance

Ecological models usually take growth rate fitness as the essential driver of population dynamics. However, as a widespread natural phenomenon, population expansion in space (or range expansion) is often governed by both motility and growth. Microbial communities offer unique systems to study how an individual's motility contributes to space competition among heterogeneous microbial populations during range expansion. Here we show that motility heterogeneity can promote the spatial segregation of subpopulations in structured microbial communities via a dynamic motility selection mechanism. Our findings are relevant to microbial stress response and microbial ecology. The results may also provide new insight to range expansion in other biological systems, such as tumor invasion and collective stress tolerance of cancer cells in densely packed environments.

Author contributions: W.Z. and Y.W. designed research; W.Z. performed research; W.Z. and Y.W. contributed new reagents/analytic tools; W.Z. and Y.W. analyzed data; and Y.W. wrote the paper.

The authors declare no competing interest.

This article is a PNAS Direct Submission.

Published under the PNAS license.

[1]To whom correspondence may be addressed. Email: ylwu@cuhk.edu.hk.

This article contains supporting information online at https://www.pnas.org/lookup/suppl/doi:10.1073/pnas.1917789117/-/DCSupplemental.

Downloaded at THE CHINESE UNIV HONG KONG on February 18, 2020

Results

Spatial Segregation of Subpopulations with Different Motilities in the Swarm. To investigate the effect of motility heterogeneity on space competition during microbial range expansion, we chose to work with *Escherichia coli*, a model bacterium displaying robust swarming behavior on agar surfaces. Swarming is a specialized form of surface translocation exhibited by many flagellated bacterial species (20–22). Cells in a bacterial swarm move actively in quasi-two-dimensional (2D) fluidic environment (24–29) and they do not perform chemotaxis (30), so swarms provide a unique system to investigate how motility per se affects population structure during range expansion. As *E. coli* strains with swarming capability but with variable speed are not available, we used antibiotic treatment to artificially induce motility heterogeneity in *E. coli* swarms. Specifically, we subjected *E. coli* cells to the stress of the aminoglycoside drug kanamycin (KAN) that collaterally reduces flagellar motility (31–33) (*SI Appendix*, Fig. S1). We grew *E. coli* swarms on antibiotic-gradient agar plates; in such an agar plate, half of the plate was infused with a linear gradient of KAN (concentration gradient: 12.5 $\mu g \cdot mL^{-1} \cdot cm^{-1}$) while the other half was left drug-free (Fig. 1*A*, *SI Appendix*, Fig. S2, and *Methods*). A mixture of two *E. coli* populations, one having genetically encoded KAN resistance (labeled by green fluorescent protein, GFP) and the other sensitive to KAN (labeled by red fluorescent protein, Katushka2S), was inoculated onto the drug-free side of such gradient plates at an initial population ratio 1:10 (Fig. 1*A*, *SI Appendix*, Fig. S2, and *Methods*). The two strains have no motility difference in a drug-free environment. Upon encountering KAN stress, however, the KAN-sensitive population will have a lower average speed than the KAN-resistant population, and the swarm will display motility heterogeneity.

Using fluorescence microscopy (*Methods*), we found that the colony swarmed as a homogeneous mixture of the two populations until reaching the region infused with KAN; then, the subpopulation with higher average speed (i.e., KAN-resistant) started to occupy a higher population proportion near the advancing edge of the swarm. After the swarm had entered the KAN-infused region for a distance of ∼25 mm (or for a duration of ∼3 h), the proportion of the higher-speed subpopulation reached up to ∼100% at the swarm edge, and the enrichment (or spatial segregation) of this subpopulation was apparent within a distance of ∼10 mm away from the edge (Fig. 1 *B* and *D*). We lowered the initial ratio between KAN-resistant and KAN-sensitive cells down to 1:100, and similar population segregation near the swarm edge was observed (*SI Appendix*, Fig. S3). This spatial segregation cannot be attributed to growth rate difference between the two subpopulations, because the growth rate advantage of KAN-resistant cells under similar KAN stress merely increased its proportion by onefold (from 10 to ∼20%), as revealed by control experiments with cells grown on nonswarming hard agar plates with the same KAN gradient for 3 h (Fig. 1 *C* and *D*). Instead, the spatial segregation is presumably a result of motility difference between the two subpopulations in the swarm. Using another aminoglycoside drug, gentamicin, that also collaterally reduces flagellar motility to induce motility heterogeneity in *E. coli* swarms, we found similar growth-independent segregation of the higher-speed subpopulation near the swarm edge (*SI Appendix*, Fig. S4). Intuitively the subpopulation with higher average speed should migrate faster toward the colony's advancing edge and thus accumulate there. However, the situation is more complicated: The colony edge advances at a speed of ∼2 to 3 μm/s, which is much slower than the mean speed of all cells (∼20 to 30 μm/s, taking the subpopulation with lower average speed into account), so all cells at the edge would have sufficient time to explore the newly available space. If we consider the extreme case where the colony edge is not moving at all, a mixed population with different motilities would remain homogeneous everywhere [except within several cell body lengths from the edge

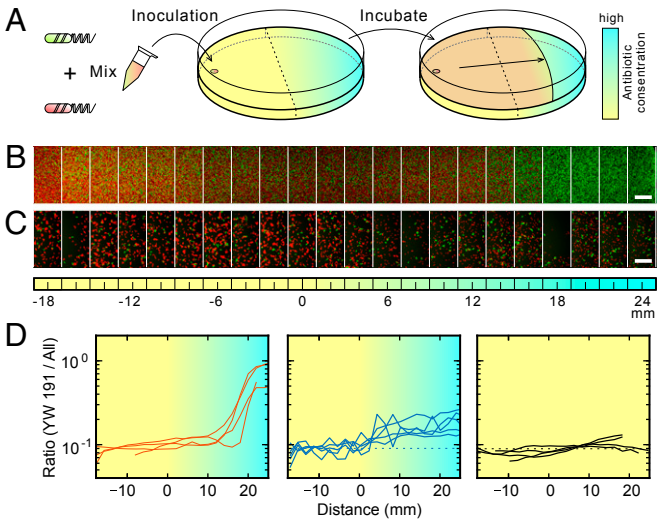

Fig. 1. Spatial segregation of subpopulations with motility heterogeneity in *E. coli* swarms. (*A*) Illustration of the protocol to induce motility heterogeneity in *E. coli* swarms on an antibiotic gradient plate. *E. coli* YW191 cells (KAN-resistant, labeled by GFP) and YW263 (KAN-sensitive, labeled by Katushka2S) were mixed and inoculated onto the drug-free side of a KAN gradient plate (*SI Appendix*, Fig. S2 and *Methods*). The dashed line on the plate marks the boundary between drug-free and drug-infused regions on the plate, and the color scale indicates relative KAN concentration. The spatial distribution of both subpopulations was measured by fluorescence microcopy along the swarm expansion direction (indicated by the black straight arrow) when the swarm had entered the KAN gradient for ∼25 mm. (*B*) Representative fluorescent image sequence showing the enrichment of the higher-speed subpopulation (YW191, green) near the swarm edge. Red fluorescence was from YW263 cells that had a smaller average speed than YW191 in the drug-infused region of KAN-gradient swarm plates. (*C*) Representative fluorescent image sequence showing the spatial distribution of YW191 (green) and YW263 (red) cells grown on nonswarming hard agar plates with the same KAN gradient as in *B*. The image sequences in *B* and *C* were taken at different locations whose relative distance to the starting position of the KAN gradient is specified by the ruler below panel C (unit: millimeters; KAN concentration increases from left to right). (Scale bars, 0.1 mm.) (*D*) Proportion of YW191 cells in swarms on KAN-gradient plates (*Left*) and in colonies on nonswarming hard agar plates (*Middle*) plotted against distance to the starting point of the KAN gradient. The population proportion (i.e., ratio between YW191 cell number and total cell number) was measured based on the fluorescence microscopy images as shown in *B* or *C* (*Methods*). The proportion of YW191 cells in swarms on antibiotic-free plates is shown for comparison (*Right*; distance = 0 mm is located at the plate center). Each line in the plots represents data from an independent colony.

(34)]. In addition, cells are densely packed in the swarm and they move erratically due to frequent collisions, with a mean free path (i.e., the average distance traveled by cells between successive abrupt turns) of just a few tens of micrometers. Therefore, it is nontrivial for the higher-speed subpopulation to migrate persistently outward and get enriched near the swarm edge.

Speed-Dependent Outward Motion Bias Enables Population Segregation via Dynamic Motility Selection. To clarify whether and how motility heterogeneity may contribute to the population segregation in a swarm, we quantified the motion pattern of single cells in swarms that were undergoing the process of population segregation. For the convenience of single-cell tracking, we mixed wild-type *E. coli* cells (nonfluorescent and KAN-sensitive) with 0.2% GFP-labeled KAN-resistant cells and 0.5% Katushka2S-labeled KAN-sensitive cells and inoculated the mixture on KAN gradient plates as described in Fig. 1*A*. We chose to track cells at ∼5 mm from the swarm edge when the swarm had entered the drug-infused region

Downloaded at THE CHINESE UNIV HONG KONG on February 18, 2020

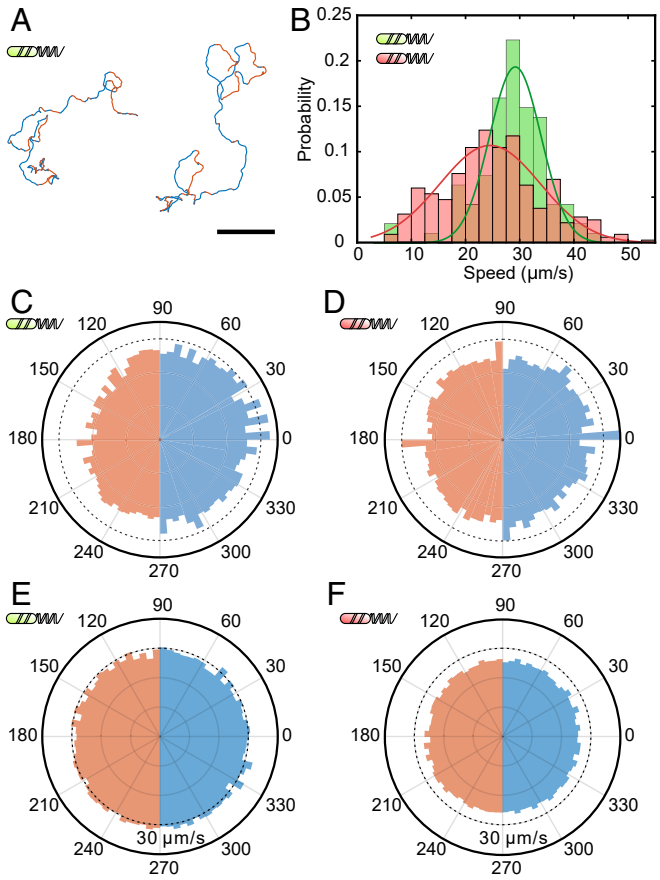

Fig. 2. Motion pattern of *E. coli* swarm cells during the spatial segregation of subpopulations with motility heterogeneity. (*A*) Representative trajectories of the higher-speed subpopulation (YW191) at ~5 mm from the swarm edge. The portions of the trajectories moving toward and away from the swarm edge are colored in blue and brown, respectively. (*B*) Speed distribution of the faster (YW191, green, $n = 94$) and the slower (YW263, red, $n = 314$) subpopulations. Lines are Gaussian fits to the speed distributions to obtain the mean and SD of population speed used in main text. (*C* and *D*) Angular probability distribution of single-cell velocity directions for the faster (*C*) and the slower (*D*) subpopulations, respectively. To generate these plots, single-cell trajectories were divided into 1-s segments and the average velocity direction of these segments was computed as an angle ranging from 0° to 360°, with the swarm expansion direction set as degree 0. The obtained velocity directions were then grouped into 80 polar angle bins of a full circle (360°), with each bin covering an angle of 4.5°. The radii of colored circular sectors in *C* and *D* are proportional to the normalized count in the corresponding angle bin and thus represent the probability of single-cell velocity directions falling within the bin. The radius of the dashed circle in each plot indicates a probability of 0.015. (*E* and *F*) Average speed of cells plotted against velocity direction for the faster (*E*) and the slower (*F*) subpopulations, respectively. In the plots of *E* and *F* the polar angle was divided into 80 bins in a way similar to *C* and *D*. Single-cell trajectories were divided into 1-s segments and for a specific polar angle bin the average speed of all trajectory segments whose velocity direction fell within this bin was computed. The radii of colored circular sectors in *E* and *F* are proportional to the average speed of cells computed for the corresponding polar angle bin, with the radius of the dashed circle indicating a speed of 30 μm/s. Blue and brown colors in *C*–*F* indicate moving toward and away from the swarm edge, respectively.

for a distance of ~15 mm (Fig. 2*A* and *Methods*). As expected, we found that the average speed of KAN-resistant subpopulation (28.7 ± 6.5 μm/s, mean ± SD, $n = 94$ cells) was higher than that of the KAN-sensitive subpopulation (25.3 ± 9.2 μm/s, mean ± SD, $n = 314$ cells; Fig. 2*B*). At this time, the enrichment of the higher-speed subpopulation (i.e., KAN-resistant cells) had started but not stabilized yet, as inferred from the modest increase of the proportion of this subpopulation (*SI Appendix*, Fig. S5). By examining the distribution of the probability for cells taking specific velocity directions, we found that the subpopulation with higher average speed tended to move outward toward the swarm edge (Fig. 2*C*, sectors in blue) rather than moving inward toward the colony center (Fig. 2*C*, sectors in brown); the subpopulation with lower average speed displayed an outward bias in velocity direction as well, but to a lesser extent (Fig. 2*D*). We note that the speed (i.e., velocity magnitude) distribution was nearly isotropic (i.e., identical in all directions) for both subpopulations (Fig. 2 *E* and *F*). The outward directional bias revealed here underlies the outward drift in collective cellular velocity reported in *E. coli* swarms (27).

To further quantify the directional bias toward swarm edge revealed above, we segmented the complete trajectory of any given cell into outward-moving and inward-moving traces. We found that the duration of these segmented traces was well-fitted by exponential distribution (Fig. 3), suggesting that cells determined randomly the duration of moving inward or outward. In agreement with the directional bias shown above, the fitted mean duration of outward-moving traces (denoted as outward persistence time, τ_{out}; *Methods*) was larger than that of inward-moving traces (denoted as inward persistence time, τ_{in}) (Fig. 3). For example, the subpopulation with higher average speed in the colony analyzed in Fig. 2 had a τ_{out} of 0.45 s versus a τ_{in} of 0.36 s; a similar observation was made with the subpopulation with lower average speed in the colony, although the difference between τ_{out} and τ_{in}

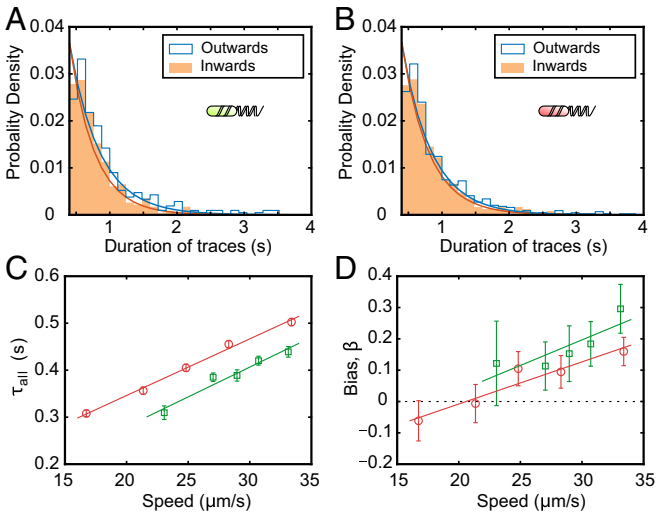

Fig. 3. Persistence time analysis for single-cell motion in *E. coli* swarms during the spatial segregation of subpopulations with motility heterogeneity. (*A* and *B*) Probability distribution of the duration of outward-moving traces (empty blue columns) and inward-moving traces (filled brown columns) for the faster (YW191; *A*) and the slower (YW263; *B*) subpopulations, respectively. Lines represent plots of exponential fit of trace duration distribution in the form of $f(t) = (1/\tau)*\exp(-t/\tau)$, with the persistence time τ being either τ_{out} or τ_{in} (i.e., the outward or the inward persistence time). τ was obtained by fitting the corresponding cumulative probability distributions to $F(t) = 1 - \exp(-t/\tau)$ (*Methods*), with the values given as follows: For YW191, $\tau_{out} = 0.45$ s, $\tau_{in} = 0.36$ s; for YW263, $\tau_{out} = 0.43$ s, $\tau_{in} = 0.39$ s. (*C*) Overall persistence time (τ_{all}) plotted as a function of cell speed for the faster (YW191, green square) and the slower (YW263, red circle) subpopulations. Lines are linear fits to the data, with R^2 being 0.95 and 0.99 for YW191 and YW263 cells, respectively. (*D*) The outward bias of persistence time (β) plotted as a function of cell speed for the faster (YW191, green square) and the slower (YW263, red circle) subpopulations. Lines are linear fits to the data, with R^2 being 0.71 and 0.91 for YW191 and YW263 cells, respectively. Error bars in *C* and *D* represent the error introduced by temporal uncertainty of single-cell tracking (*Methods*).

Downloaded at THE CHINESE UNIV HONG KONG on February 18, 2020

was smaller (0.43 s versus 0.39 s). Remarkably, for cells within the same subpopulation, the fitted mean duration of all traces used in obtaining τ_{out} and τ_{in} regardless of the moving direction (denoted as overall persistence time, τ_{all}; *Methods*) and the outward bias of persistence time [defined as $\beta = (\tau_{out} - \tau_{in})/\tau_{all}$] both increased linearly with cell speed (Fig. 3). This result is unexpected, because cells in a specific location of the swarm should "see" the same environmental cues regardless of their speeds, and it suggests that the way cells interact with their neighbors in a densely packed swarm is speed-dependent.

The speed dependence of persistence time bias enables a dynamic selection for motility advantage in the swarm: The outward drift of cells with mean speed v is $V_d \propto \beta v$; since the persistence time bias $\beta \propto v$, we have $V_d \propto v^2$, so cells with higher speeds (such as the KAN-resistant population in a swarm under KAN stress) will spend longer times moving toward the colony advancing edge with higher drift speed, leading to their accumulation at the edge. Nonetheless, faster cells would have a higher outward drift speed and thus tend to accumulate at the swarm edge, as long as the persistence time bias β is a positive constant. To discern the contribution of the speed dependence of the persistence time bias to population segregation, we express the linear relation between β and the normalized speed v in the form $\beta = kv - b$, where b and k are constants. Taking $v = 1$ as equivalent to the maximal speed 50 μm/s, the linear fits for the β–v relation in Fig. 3*D* yields $k \approx 1$ and $b \approx 0.4$ for *E. coli* swarm cells. We denote the mean speed of swarm cells ~30 μm/s as v_0 (i.e., $v_0 \approx 0.6$) and the persistence time bias at v_0 as β_0 (i.e., $\beta_0 \approx 0.2$). Any deviation of cell speed v from v_0 (denoted as $\Delta v = v - v_0$) will lead to a change in the persistence time bias (denoted as $\Delta\beta = \beta - \beta_0$) as well as a change in the population drift speed ΔV_d. Taking the derivative on both sides of $V_d \propto \beta v$ and noting that $\Delta\beta = k\Delta v$, we have $\Delta V_d = \beta_0 \Delta v + v_0 \Delta\beta = \beta_0 \Delta v + v_0 k \Delta v$, with the first term on the right-hand side contributed by the single-cell speed alone and the second term contributed by the speed-dependent bias. Since $v_0 k \approx 0.6$ and $\beta_0 \approx 0.2$, the contribution of β to the variation of V_d is approximately three times ($\sim 0.6\Delta v$) as large as that of single-cell speed ($\sim 0.2\Delta v$). Therefore, the speed dependence of persistence time bias lies at the heart of the dynamic motility selection process and it is the primary cause of the efficient spatial segregation of subpopulations with different motilities in a swarm.

The Speed-Dependent Motion Bias Is Present in Generic *E. coli* Swarms. In the above studies we had used antibiotic stress to artificially induce motility heterogeneity between subpopulations in a swarm. In fact, motility heterogeneity naturally exists in isogenic bacterial populations (as is evident from the broad speed distributions in Fig. 2*B* and *SI Appendix*, Fig. S1), and such behavioral variability among genetically identical cells may result from a variety of mechanisms (35–38). We sought to examine whether the single-cell motion pattern revealed in swarms with artificially induced motility heterogeneity is also present in generic swarming colonies with intrinsic motility heterogeneity. For this purpose we grew *E. coli* swarms on drug-free agar plates and analyzed the motion of fluorescently labeled individual cells in the swarm (*Methods*). Similar to the motion pattern presented in Fig. 3, We found that the speed distribution of cells was isotropic and the cells had a greater probability of moving outward toward the swarm edge than moving inward (Fig. 4 *A* and *B*), with the outward persistence time τ_{out} being greater than the inward persistence time τ_{in} (Fig. 4*C*). Moreover, both τ_{all} and β defined above appeared to increase linearly with cell speed (Fig. 4*D*). These results suggest that the speed dependence of persistence time bias (and thus the dynamic motility selection) is an inherent property of generic *E. coli* swarms. When the swarm edge was diluted by external liquid, we found that those isolated, noninteracting cells swimming near the diluted swarm edge did not display persistence time bias anymore (Fig. 4 *C*, *Inset*). Therefore the persistence time bias depends on physical interaction between closely packed motile cells (*Discussion*).

Dynamic Motility Selection Contributes to Collective Drug Tolerance of Swarming Colonies. Motivated by our finding that cells in generic *E. coli* swarms display speed-dependent motion bias (Fig. 4), we envision that the dynamic motility selection may provide a unique means for swarming colonies to cope with environmental stresses that collaterally reduce cell motility. When a swarming colony encounters such environmental stresses, subpopulations with transient tolerance to the stress would naturally arise in the swarm, as cell-to-cell variability of stress tolerance is widespread in bacterial populations (39–43). These stress-tolerant subpopulations have higher motility than stress-sensitive cells and thus are subject to the dynamic motility selection process; consequently, they would be enriched to the propagation front and protect the expanding colony from the stress. As a proof of concept, we sought to examine the population structure of *E. coli* swarms in response to KAN stress that reduces flagellar motility (31–33) (*SI Appendix*, Fig. S1). We grew swarms of wild-type *E. coli* (without genetically encoded KAN resistance) on KAN

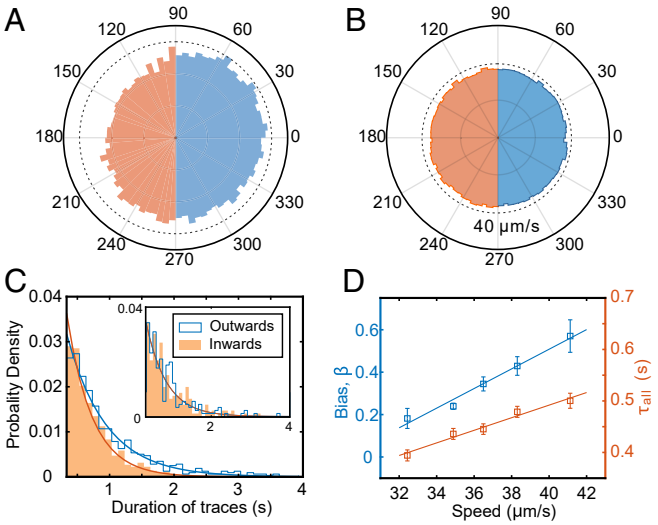

Fig. 4. Motion pattern and persistence time analysis for wild-type *E. coli* swarm cells on drug-free agar plates. (*A*) Angular probability distribution of single-cell velocity directions. The plot was generated in the same manner as done for Fig. 2 *C* and *D*. The polar angle (as a measure of single-cell velocity direction) was divided into 80 bins, and the radii of colored circular sectors in the polar plot are proportional to the probability of single-cell velocity directions falling within the corresponding polar angle bin. The radius of the dashed circle corresponds to a probability of 0.015. The swarm expansion direction is set as degree 0. (*B*) Average speed of cells plotted against velocity direction. The plot was generated in the same manner as done for Fig. 2 *E* and *F*. The radii of colored circular sectors in the polar plot are proportional to the average speed of cells computed for the corresponding polar angle bin, with the radius of the dashed circle indicating a speed of 40 μm/s. Blue and brown colors in *A* and *B* indicate moving toward and away from swarm edge, respectively. (*C*) Probability distribution of the duration of outward-moving traces (empty blue columns) and inward-moving traces (filled brown columns). Lines represent exponential fit of trace duration distribution in the form of f(t) = (1/τ)*exp(−t/τ), with the persistence time τ being either τ_{out} or τ_{in} and obtained in the same way as in Fig. 3: τ_{out} = 0.59 ± 0.01 s, τ_{in} = 0.39 ± 0.01 s. (*Inset*) Trace-duration distributions for noninteracting cells swimming near the diluted swarm edge do not show persistence time bias (both τ_{out} and τ_{in} are 0.52 s). (*D*) The overall persistence time (τ_{all}, circle) and the outward bias of persistence time (β, square) plotted as a function of cell speed. Error bars represent the error introduced by temporal uncertainty of single-cell tracking (*Methods*). Lines are linear fits to the data, with R^2 for τ_{all} and β being 0.98 and 0.84, respectively.

Downloaded at THE CHINESE UNIV HONG KONG on February 18, 2020

gradient agar plates as described previously. When such a swarm entered the KAN-infused region, it did not cease expansion until reaching ∼25 mm inside the drug-infused region (where the KAN concentration is ∼28 μg/mL, i.e., ∼3.5 times the minimum inhibitory concentration of wild-type planktonic cells) (*SI Appendix*, Figs. S6 and S7), demonstrating that the swarm had collective tolerance to KAN, in agreement with earlier reports (44–47). We measured cell survival rate in regions of lethal KAN concentrations at 3 h after the swarm ceased expansion, such that the cells would not further change their positions. Consistent with our hypothesis above, we found that the edge of those colonies was enriched with KAN-tolerant cells. In particular, cells harvested from the ∼10-mm rim of the swarm edge (i.e., in between ∼15 mm and ∼25 mm inside the KAN gradient of swarm plates) displayed a survival rate approximately two to three orders of magnitude higher than counterparts that had been grown on nonswarming agar and exposed to similar KAN stress (i.e., located in between ∼15 mm and ∼25 mm inside the KAN gradient of 1.5% hard agar plates) (Fig. 5; see schematics of the experimental protocols and additional results in *SI Appendix*, Fig. S8 and *Methods*). These KAN-tolerant cells were not persisters (48), because they were highly motile and able to sustain colony expansion; also, they were not mutants, because their KAN tolerance was transient and nonheritable (*SI Appendix*, Fig. S7). Instead, they most likely arose from the intrinsic variability of transient KAN susceptibility (40, 43), as demonstrated by the long tail in the speed distribution of wild-type cells under KAN stress (Fig. 2*B*). Although we could not distinguish and track different subpopulations in the swarm due to the lack of in situ reporters of KAN tolerance level, these KAN-tolerant cells must have been enriched toward the swarm edge via the generic dynamic motility selection process. In general, the spatial segregation of drug-tolerant subpopulations may sustain colony expansion into territories with lethal drug concentrations and confer drug tolerance to the entire swarm.

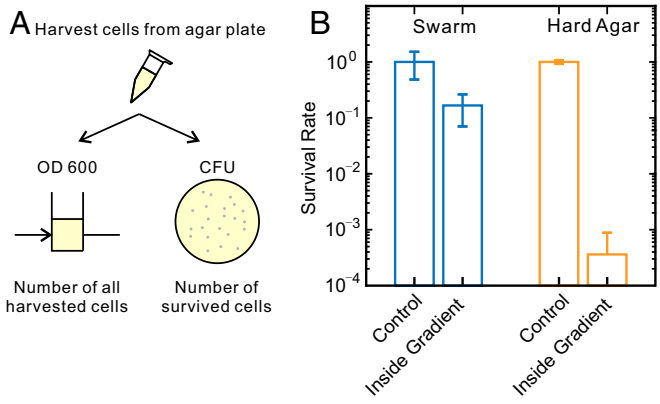

Fig. 5. Cells near the edge of *E. coli* swarms that encountered KAN stress displayed KAN tolerance. (*A*) Workflow of cell survival rate measurement. Wild-type cells were inoculated on the drug-free region of the KAN-gradient swarm plates and of the hard agar plates (that do not support swarming) (*SI Appendix*, Fig. S2 and *Methods*). Cells located in between ∼15 mm and ∼25 mm inside the KAN gradient were harvested either from the swarm plates at 3 h after the swarm had ceased expansion or from the hard agar plates after 3 h of incubation. The harvested cells were then subjected to CFU and OD_{600} measurements, and the ratio of the deduced cell numbers was taken as cell survival rate (*Methods*). (*B*) Results of cell survival rate measurement. The survival rate of cells harvested from KAN-gradient swarm plates was 0.16 ± 0.09 (blue column, Inside Gradient), with the survival rate of cells harvested from drug-free swarm plates as the control (blue column, Control). For comparison, the survival rate of cells harvested from KAN-gradient hard agar plates was $(4 \pm 5) \times 10^{-4}$ (orange column, Inside Gradient), with the survival rate of cells harvested from drug-free hard agar plates as the control (orange column, Control). Each column presents data of 6 to 21 measurements from three or more independent experiments, and error bars represent SD. Also see *SI Appendix*, Fig. S8.

Discussion

In this study we reveal that motility heterogeneity promotes the spatial segregation of subpopulations in *E. coli* swarms via a dynamic motility selection process. The dynamic motility selection is enabled by speed-dependent persistence time bias of single-cell motion, which arises from physical interaction between cells in the densely packed swarm. We further showed that, when an *E. coli* swarm encounters aminoglycoside stress that collaterally reduces cell motility, drug-tolerant subpopulations in the swarm were segregated to the advancing edge, presumably via the dynamic motility selection process. This spatial segregation of stress-tolerant subpopulations presents a unique strategy of adaptive stress response in swarming colonies.

Our results may be generally applicable to space competition process in swarms of flagellated bacteria. Indeed, we performed experiments with swarms of another flagellated bacterium, *Serratia marcescens*, and found that *S. marcescens* swarm cells display a motion pattern similar to that of *E. coli* (*SI Appendix*, Fig. S9). Although our study is focused on flagellated bacteria, it would be intriguing to examine whether the dynamic motility selection mechanism contributes to range expansion of bacterial species with other types of motility, such as *Myxococcus xanthus* with gliding motility (49) and *Pseudomonas aeruginosa* mutants powered by type IV pilus motility (13, 50).

Ecological models usually take growth rate fitness as the essential driver of population dynamics. Our results illustrate that motility heterogeneity, or "motility fitness," can play a greater role than growth rate fitness in determining the short-term spatial structure of expanding populations. In principle, our results on the empirical relation between cell speed and persistence time bias may be applied to build mathematical or computational models that are able to predict the outcome of space competition between any two mutants belonging to the same species of flagellated bacteria, provided that the factors controlling the speed of range expansion (i.e., the colony expansion rate) are known. The colony expansion rate is primarily determined by single-cell speed and growth rate, but it could also depend on certain environmental factors specific to the species concerned, such as the physical properties of growth substrate. The short-term population structure driven by dynamic motility selection may affect the long-term evolution dynamics of microbial communities. For instance, the spatial segregation of subpopulations with transient, nonheritable drug tolerance during bacterial swarming may impact the fixation dynamics and spatial structure of heritable drug resistance as the swarming colonies transit to sessile biofilms.

Resembling the early stage of biofilm formation, bacterial swarming is related to bacterial colonization in partially saturated environments and to the establishment of bacterial infections (51, 52). The finding that dynamic motility selection drives population segregation in swarms will advance our understanding of bacterial ecology and pathogenesis. In particular, bacterial swarms are known to have elevated tolerance to various antibiotics (44–47, 53–55). Altruistic cell death was thought to protect the swarming colony from antibiotic stress by releasing drug-binding targets or drug-degrading enzymes during cell lysis (47, 56). Nonetheless, certain drugs such as KAN do not cause immediate lysis when killing cells (57), so the transient collective drug tolerance of swarms to those drugs must be due to different mechanisms. The segregation of subpopulations with transient drug tolerance to the colony edge via dynamic motility selection provides a unique perspective to understand the collective drug tolerance of swarming colonies.

Our results suggest that the dynamic motility selection is an inherent property of generic *E. coli* swarms and independent of

Downloaded at THE CHINESE UNIV HONG KONG on February 18, 2020

specific types of environmental stresses. Therefore, it may serve as a general means for bacterial swarms to cope with environmental stresses that cause a collateral effect on flagellar motility. To further understand this type of adaptive stress response, it becomes necessary to examine the collateral effect of antibiotics or environmental stresses on flagellar motility, either applied alone or in combination. Such information will help to design appropriate strategies to circumvent the motility-mediated collective stress tolerance and prevent the emergence of drug resistance (48, 56, 58–63). For example, a drug having a collateral effect on flagellar motility could be used in combination with another chemical that antagonizes the motility inhibition effect [e.g., molecules blocking the pathway of DsrA to H-NS regulation (33)], thereby reducing the collective drug tolerance of the entire colony. Moreover, the dynamic motility selection offers *E. coli* swarms an efficient means to segregate different phenotypes, provided that the desired phenotype is naturally associated with higher motility or can be genetically engineered to be coupled with motility regulation.

The dynamic motility selection results from the outward, speed-dependent persistence time bias of single-cell motion. We found that the persistence time bias requires physical interaction between motile cells in a dense swarming colony (Fig. 4 *C*, *Inset*). However, the detailed mechanism is unclear yet. The speed dependence of persistence times suggests that cells with greater propulsive force can steer through a dense crowd of neighboring cells with less difficulty. Both steric and hydrodynamic interactions between cells in the swarm (26, 64, 65) may contribute to this effect. On the other hand, the reason for the persistence time biasing outward is also nontrivial. Intuitively it must be due to the outward expansion of the entire swarm. Indeed, when two swarms advancing in opposing directions merge with each other and consequently their advancing boundaries suddenly vanished, the outward bias at the merging area diminished to nearly zero within 10 min (*SI Appendix*, Fig. S10). However, as pointed out earlier, cells move erratically in the densely packed swarm due to frequent collisions, with a mean free path of just a few tens of micrometers. How can individual cells sense the outward direction when they are ∼10 mm away from the swarm advancing edge? Nutrient gradient in the growth substrate established by the swarm unlikely provides the cue. As shown by the data in Fig. 4 *C*, *Inset*, when the swarm edge was diluted by a small amount of external liquid (which equilibrated with the nutrient level in growth substrate quickly and presumably did not perturb the nutrient gradient in agar), those isolated and noninteracting cells swimming near the diluted swarm edge did not display persistence time bias anymore, despite that the nutrient gradient in agar must be still present. The expansion of the swarm as a whole somehow provides a long-range cue for individual cells, which is likely an emergent effect due to collective physical interactions between cells. Elucidating the detailed mechanism accounting for the outward and speed-dependent persistence time bias may provide insights for the control of collective motion and phase separation in general self-propelled particle systems (34, 66–70).

Methods

Bacterial Strains. The following strains were used: *E. coli* HCB1737 (a derivative of *E. coli* AW405 with wild-type swarming behavior and sensitive to β-lactams, aminoglycosides, and fluoroquinolones, referred to as wild type, a gift from Howard Berg, Harvard University, Cambridge, MA); YW191 [*E. coli* HCB1737 transformed with pAM06-tet plasmid carrying KAN resistance and expressing GFP constitutively; the pAM06-tet plasmid was a gift from Arnab Mukherjee and Charles M. Schroeder, University of Illinois at Urbana–Champaign, Urbana, IL (71)]; YW263 (*E. coli* HCB1737 transformed with the plasmid pKatushka2S-B [FP763; Evrogen] carrying CAR resistance and expressing red fluorescent protein Katushka2S constitutively); YW354 (*E. coli* HCB1737 transformed with a plasmid carrying GENT resistance and expressing Katushka2S constitutively); *S. marcescens* ATCC 274; and *S. marcescens* ATCC 274 transformed with the plasmid pKatushka2S-B. Plasmids were transformed via electroporation. Single-colony isolates were grown overnight (∼13 to 14 h) with shaking in LB medium (1% Bacto tryptone, 0.5% yeast extract, and 0.5% NaCl) at 30 °C to stationary phase. For YW191, YW263, and YW354, antibiotic (KAN 50 μg/mL, carbenicillin 50 μg/mL, and gentamicin 50 μg/mL) was added to the growth medium for maintaining the plasmid. Overnight cultures were used for inoculating swarm plates.

Agar Plates without Antibiotics. To prepare antibiotic-free swarm plates, swarm agar (0.6% Eiken agar infused with 1% Bacto peptone, 0.3% beef extract, and 0.5% NaCl) was autoclaved and stored at room temperature. Before use, the agar was melted in a microwave oven, cooled to ∼60 °C, and pipetted in 10-mL aliquots into 90-mm polystyrene Petri plates. The plates were swirled gently to ensure surface flatness and then cooled for 5 min without a lid inside a large Plexiglas [poly(methyl methacrylate), PMMA] box. Antibiotic-free hard agar plates were prepared in a similar manner, except that 1.5% Eiken agar concentration was used. For the swarm plates, drops of diluted (10^{-2}) overnight bacterial cultures (1 μL; described above) were inoculated at a distance of 1 cm from the edge of the plates. The swarm plates were dried for another 10 min without a lid, covered, and incubated at 30 °C and ∼95% relative humidity for desired durations of time. For the hard agar plates, overnight *E. coli* culture was diluted 10^{-2} in fresh LB medium and incubated at 30 °C with shaking (180 rpm) for 3 h to exponential phase (optical density at 600 nm, OD_{600} ∼0.5). Then, the cells were concentrated by 20-fold via centrifugation (5,000 × *g*, 3 min); 100 μL of the concentrated culture was spread uniformly onto the agar surface of a plate using sterile glass beads (3 mm in diameter), and the plate was incubated at 30 °C and ∼50% relative humidity for the desired duration of time.

Antibiotic-Gradient Plate Assay. To prepare agar plates with linear antibiotic gradient, molten Eiken agar (0.6% for swarm plates and 1.5% for hard agar plates) was cooled to ∼50 °C; 5 mL of the agar was mixed with antibiotics at desired final concentrations. This antibiotic-infused agar was poured into a tilted 90-mm nonvented Petri dish (tilt angle ∼3.8°) and solidified in the PMMA box without a lid for 5 min, forming a wedge shape that covers about half of the plate. Then the plate was laid flat, and 15 mL antibiotic-free agar was poured into the plate to cover the antibiotic-infused wedge. The plate was left in the PMMA box without a lid for another 5 min. Antibiotics diffused from the wedge and a gradient of antibiotic concentration was established across half of the agar plate. Also see *SI Appendix*, Fig. S2.

For swarm-agar gradient plates, 1 μL diluted (10^{-2}) overnight *E. coli* culture as described above was inoculated on the antibiotic-free region of the plate at ∼1 cm from the edge of the Petri dish. The plate was dried for 10 min in the PMMA box without a lid. Then, the plate was incubated at 30 °C and ∼95% relative humidity for desired durations of time. For hard agar gradient plates, the plates were prepared as described above at 3 h before inoculating cells. The plates were dried under laminar flow for 20 min and subsequently kept in an incubator at 30 °C and ∼50% relative humidity. To inoculate hard agar gradient plates, 100 μL concentrated bacterial culture (as described above) was spread uniformly on the agar surface of a plate with sterile 3-mm glass beads and the plate was incubated at 30 °C and ∼50% relative humidity for the desired duration of time.

Monitoring Swarm Expansion Dynamics. Swarm expansion dynamics was monitored and measured in a custom-built imaging incubator made of PMMA (length × depth × height, 1 × 1 × 1.2 m). The swarm plates were sealed with parafilm before incubation in order to maintain saturated humidity. The temperature of the incubator was maintained at 30 °C with a heater controlled by feedback circuits. The inner walls of the incubator were covered with black cloth and the plate was illuminated by a light-emitting diode (LED) strip lining at the bottom part of the side walls. The images of swarm plates were photographed by a digital camera (700D; Canon) every 5 min during incubation (24 mm, aperture f/8, exposure time 1/5 s). The time-lapse imaging and LED illumination were triggered by a custom-programmed microcontroller (Arduino).

Phase Contrast and Fluorescence Imaging. Imaging was performed on motorized microscopes (Nikon TI-E or Nikon NI-E). Fluorescence imaging was performed in epifluorescence using filter sets specified below, with the excitation light provided by a mercury precentered fiber illuminator (Nikon Intensilight). Recordings were made with a scientific complementary metal–oxide–semiconductor (sCMOS) camera (Andor Zyla 4.2 PLUS USB 3.0 or Andor Neo 5.5; Andor Technology). In all experiments the Petri dishes were covered with a lid to prevent evaporation and air convection, and the sample temperature was maintained at 30 °C using a custom-built temperature-control system installed on the microscope stage, unless otherwise stated.

Downloaded at THE CHINESE UNIV HONG KONG on February 18, 2020

Measurement of Population Ratio in Colonies. Overnight cultures of drug-resistant and drug-sensitive *E. coli* strains, both labeled with fluorescent proteins, were washed by centrifugation (5,000 × *g*, 3 min) and adjusted to OD_{600} ~2 with fresh LB medium. Then, the drug-resistant cells were mixed with drug-sensitive cells at specified ratios. For the swarming case, 1 μL of the cell mixture was inoculated on a swarm plate with or without antibiotic gradient, and the plate was incubated as described above. For cell growth on hard agar plates, 100 μL of the cell mixture was spread uniformly on the agar surface of a plate with sterile 3-mm glass beads, and the plate was incubated as described above. After incubation, the plates were transferred to the stage of a motorized upright microscope (Nikon NI-E). Fluorescent images of drug-resistant and drug-sensitive populations in the colony were taken by the Andor Neo sCMOS camera through a 20× objective (Nikon CFI Plan Fluor DLL 20×, numerical aperture [N.A.] 0.50, working distance [W.D.] 2.1 mm), and the following filter sets were used: an mCherry filter set for YW263 and YW354 cells labeled with the red fluorescent protein Katushka2S (excitation 562/40 nm, emission 641/75 nm, dichroic: 593 nm; mCherry-B-000; Semrock Inc.) and a fluorescein isothiocyanate (FITC) filter set for YW191 cells labeled with GFP (excitation 482/35 nm, emission 536/40 nm, dichroic: 506 nm; FITC-3540C-000; Semrock Inc.). The fluorescent images were taken every 2 mm along the swarm expansion direction (i.e., the up-gradient direction) from the antibiotic-free side to the swarm edge, and the camera exposure time was set as 20 ms for each fluorescence image. The population ratio of a subpopulation of cells was computed with a custom-written program in MATLAB based on the background-corrected fluorescence count of the fluorescent images, using the fluorescence count of cells on antibiotic-free plate or on the antibiotic-free side of the gradient plate as the reference.

Measurement of Single-Cell Speed Distribution and Motion Pattern. To measure the single-cell speed distribution of planktonic cells before and after antibiotic treatment, 10- mL overnight cultures (grown in 125-mL Erlenmeyer flasks) of drug-resistant and drug-sensitive *E. coli* strains, both labeled with fluorescent proteins, were washed by centrifugation (5,000 × *g*, 3 min) and adjusted to OD_{600} ~1 with fresh Eiken broth. The two cultures were mixed 1:1 and diluted 10^{-2} in 10 mL fresh Eiken broth. The diluted mixed culture was incubated at 30 °C with shaking (180 rpm) for 3 h to exponential phase (OD_{600} ~0.5), and then the culture was supplemented with the antibiotic at specified final concentrations and was further incubated at 30 °C with shaking (180 rpm) for desired durations of time. In the meantime, a 0.6% Eiken agar plate without antibiotics was prepared as described above. Following the antibiotic treatment, 3 μL fresh Eiken broth was deposited onto the agar surface to form a droplet, 2 μL of the antibiotic-treated planktonic culture was inoculated into the droplet, and subsequently a cover glass (25 mm × 25 mm) was gently placed onto the droplet, forming a quasi-2D liquid layer between the cover glass and the agar surface. The agar plate was then transferred to a motorized inverted microscope (Nikon Ti-E). The motion of cells dispersed in the quasi-2D liquid layer was recorded in fluorescence by the Andor Zyla sCMOS camera (20-ms exposure time, 30 frames per second [fps]) through a long-W.D. 20× objective (Nikon CFI Super Plan Fluor ELWD ADM 20XC, N.A. 0.45, W.D. 8.2 to 6.9 mm) and using the filter sets described above.

To measure the single-cell motion pattern of cells in swarms, the swarm plates were inoculated in the same manner as described above, except that overnight cultures of wild-type and fluorescently labeled strains were adjusted to OD_{600} ~2 with fresh LB medium after centrifugation (5,000 × *g*, 3 min) and then mixed at the following ratios: Wild-type *E. coli* cells were mixed with 0.2% YW191 cells and 0.5% YW263 cells to inoculate KAN-gradient swarm plates, while wild-type *E. coli* cells were mixed with 0.1% YW191 cells to inoculate antibiotic-free swarm plates. The swarm plates were incubated as described above until they had expanded for the specified distance. The swarm plates were then transferred to the stage of the microscope (Nikon Ni-E for KAN-gradient swarm plates and Nikon Ti-E for antibiotic-free swarm plates). The motion of cells in KAN-gradient swarm plates or in antibiotic-free swarm plates was recorded for 10 to 30 s in fluorescence by the Andor Neo sCMOS camera (20-ms exposure time, 25 fps) through the 20× objective or by the Andor Zyla sCMOS camera (20-ms exposure time, 30 fps) through the long-W.D. 20× objective, respectively. Filter sets described above were used.

The trajectories of cells were obtained by single-cell tracking based on the recorded videos, using a custom-written program in MATLAB. Specifically, the following image-processing algorithm was adopted 1) For each image frame, the grayscale image was transformed into a binary (black and white) image, and then the position of each fluorescently labeled cell was located by first finding the boundary of each cell (as white dots) and then computing the center of the boundary. 2) Each image was then partitioned into Thiessen (or Voronoi) polygons by the cells' location, such that each polygon contained only one cell. 3) For the partition of frames n and (n + 1), if there was one and only one cell in the same polygon for both frame n and n + 1, the two cells were taken as the same one and thus its trajectory from frame n to frame (n + 1) was obtained. 4) Iterate steps 1 through 3 for all frames to obtain the complete trajectory of all cells. The cells' trajectories were then used to analyze their swimming speed and motion pattern.

Fitting of Persistence Time. The trajectories of cells were segmented into outward-moving (moving toward the swarm edge) and inward-moving (moving away from the swarm edge) traces. Traces with duration shorter than 10 frames were discarded. The number of outward-moving traces (N_{out}) and inward-moving traces (N_{in}) in each case was as follows: For Fig. 3*A*, N_{out} = 331 and N_{in} = 304; for Fig. 3*B*, N_{out} = 662 and N_{in} = 667; for Fig. 4*C*, N_{out} = 622 and N_{in} = 686. The outward and inward persistence times (τ_{out} and τ_{in}) were obtained by least-square fitting of the cumulative distribution of the duration of these outward-moving and inward-moving traces, respectively, to the exponential distribution $F(t) = 1 - \exp(-t/\tau)$, with τ being either τ_{out} or τ_{in}. The overall persistence time τ_{all} was obtained by least-square fitting of the cumulative distribution of the duration of all traces that were used in obtaining τ_{out} and τ_{in} to the exponential distribution $F(t) = 1 - \exp(-t/\tau)$. To account for the random error in trace duration measurement, the duration of every single trace in a dataset was imposed by a noise of $\xi = 2\cdot(-1)^k$ frames, where k is an integer randomly drawn from 0 and 1 for each trace; this operation was performed on the entire trace-duration dataset for 200 times, resulting in 200 noise-modified datasets. The fitting described above was done for each of the noise-modified dataset, and the SD of the resultant persistent times was taken as the measurement error of the persistent time. The error in bias was derived from the measurement errors of the persistent times.

Survival Rate Measurement under Antibiotic Stress. To measure survival rate of *E. coli* swarm cells under antibiotic stress, cells were harvested from the swarm edge at specified locations at 3 h after the swarm had ceased expansion, by dispensing 1 mL fresh Eiken broth (1% Bacto peptone, 0.3% beef extract, and 0.5% NaCl) to the colony and then recollecting the suspended culture. To measure survival rate of cells grown on nonswarming hard agar plates under antibiotic stress, cells grown for 3 h on the plates were harvested from specified locations by dispensing 1 mL fresh Eiken broth to the plate and then recollecting the suspended culture.

After culture samples were harvested, the total number of cells in the samples (both alive and dead) was estimated by OD_{600} measurement. Note that KAN stress used in our experiments did not cause cell lysis at the time of OD_{600} measurement, so the cell number yielded from OD_{600} measurement may include dead cells. Then we performed colony-forming unit (CFU) counting for each sample to measure the number of cells that were still alive. Briefly, a culture sample was diluted to appropriate cell density (~10^4 cells per mL) and 20 μL of the diluted culture was well mixed with 4 mL molten 0.6% LB agar (at ~40 °C). The cell–agar mixture was uniformly spread onto a 1.5% LB agar plate. Then, the plate was incubated at 30 °C for ~18 h until colonies appeared. The number of colonies on the plate was counted based on plate photographs using a custom-written program in MATLAB R2014b (The MathWorks). The photographs were first transformed into binary black-and-white images by choosing a suitable threshold, and the number of white spots was counted as the CFU number. The survival rate was computed as CFU number divided by the total cell number in the diluted sample obtained by OD_{600} measurement. The computed survival rates for each growth condition were then normalized by the survival rate measured in control experiments (without antibiotic stress). For each growth condition, at least three samples (biological replicate) and at least eight CFU plates (technical replicate) were used.

Data Availability Statement. All data discussed in the paper are available in the main text and *SI Appendix*.

ACKNOWLEDGMENTS. We thank Howard C. Berg, Arnab Mukherjee, and Charles M. Schroeder for their kind gifts of bacterial strains; we thank Fan Jin, Liang Yang, and Junhua Yuan for helpful comments. During manuscript preparation we learned from Junhua Yuan and Rongjing Zhang that they had taken a similar approach to analyze single-cell motion pattern as we did for Fig. 3 *A* and *B*, but under different swarming conditions. This work was supported by the National Natural Science Foundation of China (NSFC 21473152 to Y.W.) and by the Research Grants Council of Hong Kong Special Administration Region (Ref. No. General Research Fund 14322316 to Y.W.).

Downloaded at THE CHINESE UNIV HONG KONG on February 18, 2020

1. B. L. Phillips, G. P. Brown, J. K. Webb, R. Shine, Invasion and the evolution of speed in toads. *Nature* **439**, 803 (2006).
2. N. V. Krakhmal, M. V. Zavyalova, E. V. Denisov, S. V. Vtorushin, V. M. Perelmuter, Cancer invasion: Patterns and mechanisms. *Acta naturae* **7**, 17–28 (2015).
3. B. J. Finlay, K. J. Clarke, Ubiquitous dispersal of microbial species. *Nature* **400**, 828 (1999).
4. M. E. Hibbing, C. Fuqua, M. R. Parsek, S. B. Peterson, Bacterial competition: Surviving and thriving in the microbial jungle. *Nat. Rev. Microbiol.* **8**, 15–25 (2010).
5. P. B. Pearman, A. Guisan, O. Broennimann, C. F. Randin, Niche dynamics in space and time. *Trends Ecol. Evol. (Amst.)* **23**, 149–158 (2008).
6. S. Klopfstein, M. Currat, L. Excoffier, The fate of mutations surfing on the wave of a range expansion. *Mol. Biol. Evol.* **23**, 482–490 (2006).
7. K. M. Ibrahim, R. A. Nichols, G. M. Hewitt, Spatial patterns of genetic variation generated by different forms of dispersal during range expansion. *Heredity* **77**, 282–291 (1996).
8. R. Smith *et al*., Programmed Allee effect in bacteria causes a tradeoff between population spread and survival. *Proc. Natl. Acad. Sci. U.S.A.* **111**, 1969–1974 (2014).
9. K. C. Yang, Z. X. Wu, P. Holme, E. Nonaka, Expansion of cooperatively growing populations: Optimal migration rates and habitat network structures. *Phys Rev E* **95**, 012306 (2017).
10. C. M. Jessup *et al*., Big questions, small worlds: Microbial model systems in ecology. *Trends Ecol. Evol. (Amst.)* **19**, 189–197 (2004).
11. O. Hallatschek, P. Hersen, S. Ramanathan, D. R. Nelson, Genetic drift at expanding frontiers promotes gene segregation. *Proc. Natl. Acad. Sci. U.S.A.* **104**, 19926–19930 (2007).
12. D. T. Fraebel *et al*., Environment determines evolutionary trajectory in a constrained phenotypic space. *eLife* **6**, e24669 (2017).
13. M. Deforet, C. Carmona-Fontaine, K. S. Korolev, J. B. Xavier, Evolution at the edge of expanding populations. *Am. Nat.* **194**, 291–305 (2019).
14. W. C. Allee, *The Social Life of Animals* (W W Norton & Co, New York, 1938), pp. 293.
15. L. Dai, D. Vorselen, K. S. Korolev, J. Gore, Generic indicators for loss of resilience before a tipping point leading to population collapse. *Science* **336**, 1175–1177 (2012).
16. B. T. Weinstein, M. O. Lavrentovich, W. Möbius, A. W. Murray, D. R. Nelson, Genetic drift and selection in many-allele range expansions. *PLOS Comput. Biol.* **13**, e1005866 (2017).
17. S. Fodelianakis *et al*., Dispersal homogenizes communities via immigration even at low rates in a simplified synthetic bacterial metacommunity. *Nat. Commun.* **10**, 1314 (2019).
18. H. Vlamakis, C. Aguilar, R. Losick, R. Kolter, Control of cell fate by the formation of an architecturally complex bacterial community. *Genes Dev.* **22**, 945–953 (2008).
19. H. Xu, J. Dauparas, D. Das, E. Lauga, Y. Wu, Self-organization of swimmers drives long-range fluid transport in bacterial colonies. *Nat. Commun.* **10**, 1792 (2019).
20. R. M. Harshey, Bacterial motility on a surface: Many ways to a common goal. *Annu. Rev. Microbiol.* **57**, 249–273 (2003).
21. M. F. Copeland, D. B. Weibel, Bacterial swarming: A model system for studying dynamic self-assembly. *Soft Matter* **5**, 1174–1187 (2009).
22. D. B. Kearns, A field guide to bacterial swarming motility. *Nat. Rev. Microbiol.* **8**, 634–644 (2010).
23. G. Lambert *et al*., An analogy between the evolution of drug resistance in bacterial communities and malignant tissues. *Nat. Rev. Cancer* **11**, 375–382 (2011).
24. N. C. Darnton, L. Turner, S. Rojevsky, H. C. Berg, Dynamics of bacterial swarming. *Biophys. J.* **98**, 2082–2090 (2010).
25. H. P. Zhang, A. Be'er, E.-L. Florin, H. L. Swinney, Collective motion and density fluctuations in bacterial colonies. *Proc. Natl. Acad. Sci. U.S.A.* **107**, 13626–13630 (2010).
26. Y. Wu, B. G. Hosu, H. C. Berg, Microbubbles reveal chiral fluid flows in bacterial swarms. *Proc. Natl. Acad. Sci. U.S.A.* **108**, 4147–4151 (2011).
27. Y. Wu, H. C. Berg, Water reservoir maintained by cell growth fuels the spreading of a bacterial swarm. *Proc. Natl. Acad. Sci. U.S.A.* **109**, 4128–4133 (2012).
28. J. D. Partridge, R. M. Harshey, More than motility: Salmonella flagella contribute to overriding friction and facilitating colony hydration during swarming. *J. Bacteriol.* **195**, 919–929 (2013).
29. G. Ariel *et al*., Swarming bacteria migrate by Lévy Walk. *Nat. Commun.* **6**, 8396 (2015).
30. S. Mariconda, Q. Wang, R. M. Harshey, A mechanical role for the chemotaxis system in swarming motility. *Mol. Microbiol.* **60**, 1590–1602 (2006).
31. S. Benisty, E. Ben-Jacob, G. Ariel, A. Be'er, Antibiotic-induced anomalous statistics of collective bacterial swarming. *Phys. Rev. Lett.* **114**, 018105 (2015).
32. B. W. Brunelle, B. L. Bearson, S. M. D. Bearson, T. A. Casey, Multidrug-resistant *Salmonella enterica* serovar typhimurium isolates are resistant to antibiotics that influence their swimming and swarming motility. *MSphere* **2**, e00306-17 (2017).
33. Y. Fan, C. R. Evans, J. Ling, Reduced protein synthesis fidelity inhibits flagellar biosynthesis and motility. *Sci. Rep.* **6**, 30960 (2016).
34. C. Andrea, E. Jens, A. Thorsten, G. Gerhard, R. Marisol, Motility-sorting of self-propelled particles in microchannels. *EPL* **107**, 36003 (2014).
35. E. Korobkova, T. Emonet, J. M. G. Vilar, T. S. Shimizu, P. Cluzel, From molecular noise to behavioural variability in a single bacterium. *Nature* **428**, 574–578 (2004).
36. P. S. Stewart, M. J. Franklin, Physiological heterogeneity in biofilms. *Nat. Rev. Microbiol.* **6**, 199–210 (2008).
37. D. Huh, J. Paulsson, Non-genetic heterogeneity from stochastic partitioning at cell division. *Nat. Genet.* **43**, 95–100 (2011).
38. T. M. Norman, N. D. Lord, J. Paulsson, R. Losick, Stochastic switching of cell fate in microbes. *Annu. Rev. Microbiol.* **69**, 381–403 (2015).
39. X. Wang *et al*., Heteroresistance at the single-cell level: Adapting to antibiotic stress through a population-based strategy and growth-controlled interphenotypic coordination. *MBio* **5**, e00942–13 (2014).
40. M. A. Sánchez-Romero, J. Casadesús, Contribution of phenotypic heterogeneity to adaptive antibiotic resistance. *Proc. Natl. Acad. Sci. U.S.A.* **111**, 355–360 (2014).
41. S. S. Motta, P. Cluzel, M. Aldana, Adaptive resistance in bacteria requires epigenetic inheritance, genetic noise, and cost of efflux pumps. *PLoS One* **10**, e0118464 (2015).
42. I. El Meouche, Y. Siu, M. J. Dunlop, Stochastic expression of a multiple antibiotic resistance activator confers transient resistance in single cells. *Sci. Rep.* **6**, 19538 (2016).
43. O. M. El-Halfawy, M. A. Valvano, Antimicrobial heteroresistance: An emerging field in need of clarity. *Clin. Microbiol. Rev.* **28**, 191–207 (2015).
44. W. Kim, T. Killam, V. Sood, M. G. Surette, Swarm-cell differentiation in *Salmonella enterica* serovar typhimurium results in elevated resistance to multiple antibiotics. *J. Bacteriol.* **185**, 3111–3117 (2003).
45. W. Kim, M. G. Surette, Swarming populations of Salmonella represent a unique physiological state coupled to multiple mechanisms of antibiotic resistance. *Biol. Proced. Online* **5**, 189–196 (2003).
46. S. Lai, J. Tremblay, E. Déziel, Swarming motility: A multicellular behaviour conferring antimicrobial resistance. *Environ. Microbiol.* **11**, 126–136 (2009).
47. M. T. Butler, Q. Wang, R. M. Harshey, Cell density and mobility protect swarming bacteria against antibiotics. *Proc. Natl. Acad. Sci. U.S.A.* **107**, 3776–3781 (2010).
48. K. Lewis, Persister cells. *Annu. Rev. Microbiol.* **64**, 357–372 (2010).
49. Y. Wu, A. D. Kaiser, Y. Jiang, M. S. Alber, Periodic reversal of direction allows Myxobacteria to swarm. *Proc. Natl. Acad. Sci. U.S.A.* **106**, 1222–1227 (2009).
50. M. E. Anyan *et al*., Type IV pili interactions promote intercellular association and moderate swarming of Pseudomonas aeruginosa. *Proc. Natl. Acad. Sci. U.S.A.* **111**, 18013–18018 (2014).
51. N. Verstraeten *et al*., Living on a surface: Swarming and biofilm formation. *Trends Microbiol.* **16**, 496–506 (2008).
52. B. V. Jones, R. Young, E. Mahenthiralingam, D. J. Stickler, Ultrastructure of Proteus mirabilis swarmer cell rafts and role of swarming in catheter-associated urinary tract infection. *Infect. Immun.* **72**, 3941–3950 (2004).
53. J. Overhage, M. Bains, M. D. Brazas, R. E. W. Hancock, Swarming of Pseudomonas aeruginosa is a complex adaptation leading to increased production of virulence factors and antibiotic resistance. *J. Bacteriol.* **190**, 2671–2679 (2008).
54. D. Roth *et al*., Identification and characterization of a highly motile and antibiotic refractory subpopulation involved in the expansion of swarming colonies of Paenibacillus vortex. *Environ. Microbiol.* **15**, 2532–2544 (2013).
55. J. D. Partridge, G. Ariel, O. Schvartz, R. M. Harshey, A. Be'er, The 3D architecture of a bacterial swarm has implications for antibiotic tolerance. *Sci. Rep.* **8**, 15823 (2018).
56. H. R. Meredith, J. K. Srimani, A. J. Lee, A. J. Lopatkin, L. You, Collective antibiotic tolerance: Mechanisms, dynamics and intervention. *Nat. Chem. Biol.* **11**, 182–188 (2015).
57. M. A. Kohanski, D. J. Dwyer, J. J. Collins, How antibiotics kill bacteria: From targets to networks. *Nat. Rev. Microbiol.* **8**, 423–435 (2010).
58. B. R. Levin, D. E. Rozen, Non-inherited antibiotic resistance. *Nat. Rev. Microbiol.* **4**, 556–562 (2006).
59. N. R. Cohen, M. A. Lobritz, J. J. Collins, Microbial persistence and the road to drug resistance. *Cell Host Microbe* **13**, 632–642 (2013).
60. N. M. Vega, J. Gore, Collective antibiotic resistance: Mechanisms and implications. *Curr. Opin. Microbiol.* **21**, 28–34 (2014).
61. A. Brauner, O. Fridman, O. Gefen, N. Q. Balaban, Distinguishing between resistance, tolerance and persistence to antibiotic treatment. *Nat. Rev. Microbiol.* **14**, 320–330 (2016).
62. A. C. Palmer, R. Kishony, Understanding, predicting and manipulating the genotypic evolution of antibiotic resistance. *Nat. Rev. Genet.* **14**, 243–248 (2013).
63. J. M. A. Blair, M. A. Webber, A. J. Baylay, D. O. Ogbolu, L. J. V. Piddock, Molecular mechanisms of antibiotic resistance. *Nat. Rev. Microbiol.* **13**, 42–51 (2015).
64. S. D. Ryan, G. Ariel, A. Be'er, Anomalous fluctuations in the orientation and velocity of swarming bacteria. *Biophys. J.* **111**, 247–255 (2016).
65. Y. Li, H. Zhai, S. Sanchez, D. B. Kearns, Y. Wu, Noncontact cohesive swimming of bacteria in two-dimensional liquid films. *Phys. Rev. Lett.* **119**, 018101 (2017).
66. S. Ramaswamy, The mechanics and statistics of active matter. *Annu. Rev. Condens. Matter Phys.* **1**, 323–345 (2010).
67. T. Vicsek, A. Zafeiris, Collective motion. *Phys. Rep.* **517**, 71–140 (2012).
68. P. Romanczuk, M. Bär, W. Ebeling, B. Lindner, L. Schimansky-Geier, Active brownian particles. *Eur. Phys. J. Spec. Top.* **202**, 1–162 (2012).
69. S. R. McCandlish, A. Baskaran, M. F. Hagan, Spontaneous segregation of self-propelled particles with different motilities. *Soft Matter* **8**, 2527–2534 (2012).
70. C. Chen, S. Liu, X. Q. Shi, H. Chaté, Y. Wu, Weak synchronization and large-scale collective oscillation in dense bacterial suspensions. *Nature* **542**, 210–214 (2017).
71. A. Mukherjee, J. Walker, K. B. Weyant, C. M. Schroeder, Characterization of flavin-based fluorescent proteins: An emerging class of fluorescent reporters. *PLoS One* **8**, e64753 (2013).

Downloaded at THE CHINESE UNIV HONG KONG on February 18, 2020